ISSN 1560-3547, Regular and Chaotic Dynamics, 2014, Vol. 19, No. 4, pp. 483–494. © Pleiades Publishing, Ltd., 2014.

Attractor of Smale – Williams Type in an Autonomous Distributed System

Vyacheslav P. Kruglov[1,2*], Sergey P. Kuznetsov[1,3], and Arkady Pikovsky[2***]**

[1] *Saratov State University, ul. Astrakhanskaya 83, Saratov, 410012 Russia*

[2] *Department of Physics and Astronomy, University of Potsdam, Karl-Liebknecht-Str. 24/25, D-14476 Potsdam-Golm, Germany*

[3] *Kotel'nikov's Institute of Radio-Engineering and Electronics of RAS, Saratov Branch, ul. Zelenaya 38, Saratov, 410019 Russia*

Received January 30, 2014; accepted February 18, 2014

Abstract—We consider an autonomous system of partial differential equations for a one-dimensional distributed medium with periodic boundary conditions. Dynamics in time consists of alternating birth and death of patterns with spatial phases transformed from one stage of activity to another by the doubly expanding circle map. So, the attractor in the Poincaré section is uniformly hyperbolic, a kind of Smale – Williams solenoid. Finite-dimensional models are derived as ordinary differential equations for amplitudes of spatial Fourier modes (the 5D and 7D models). Correspondence of the reduced models to the original system is demonstrated numerically. Computational verification of the hyperbolicity criterion is performed for the reduced models: the distribution of angles of intersection for stable and unstable manifolds on the attractor is separated from zero, i.e., the touches are excluded. The example considered gives a partial justification for the old hopes that the chaotic behavior of autonomous distributed systems may be associated with uniformly hyperbolic attractors.

MSC2010 numbers: 37D45, 37D20, 35B36

DOI: 10.1134/S1560354714040042

Keywords: Smale – Williams solenoid, hyperbolic attractor, chaos, Swift – Hohenberg equation, Lyapunov exponent

1. INTRODUCTION

Uniformly hyperbolic chaotic attractors such as the Smale – Williams solenoid or Plykin attractor were introduced in the mathematical theory of dynamical systems several decades ago [1–5]. Figure 1 shows a construction of the Smale – Williams attractor: at one step a toroidal domain transforms into a narrow tube in the form of a double loop embedded inside the original domain. After many steps, asymptotically, the solenoid arises having an infinite number of turns and Cantor-like transversal structure. Once it was believed that such attractors may describe chaos and turbulence in many cases, but later it turned out that chaotic dynamics commonly occurring in applications do not fit the class of uniformly hyperbolic attractors.

Physically implementable systems with hyperbolic chaos were discovered (or, rather constructed) only very recently [6–10]. Their principle of operation was based on the chaotic nature of maps for the angular variables characterizing phases of oscillations in time, at successive stages of activity of oscillatory elements constituting the system.

An alternative general approach to the elaboration of systems with hyperbolic chaos, appropriate for spatially extended systems, was advanced in Ref. [11]: instead of phases of oscillations in time,

* E-mail: kruglovyacheslav@gmail.com

** E-mail: spkuz@rambler.ru

*** E-mail: pikovsky@uni-potsdam.de

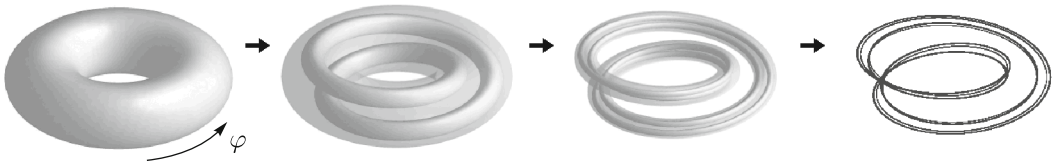

Fig. 1. An initial toroidal domain in the phase space, and results of its transformation at successive steps of discrete-time evolution, with formation of the Smale – Williams solenoid after a large number of repetitions of the mapping. The angular variable φ undergoes a double expansion at each next step.

it was suggested to deal with *spatial phases* of patterns generated in a distributed medium. In computations, this principle was demonstrated and illustrated with a model based on a modified Swift – Hohenberg equation. Due to externally forced periodic modulation of a parameter controlling the characteristic spatial scale, the model system generates long-wave and short-wave Turing patterns alternately, and operates in such a way that the spatial phases at successive stages of the dynamical evolution are governed by an expanding circle map. One more example with analogous dynamics of the spatial phases relates to alternating parametric excitation of long-scale and short-scale standing-wave patterns due to pump modulation in a medium described by a wave equation with nonlinear dissipation [12, 13]. Such examples justify, at least partially, the old expectations for applicability of the hyperbolic theory to chaotic dynamics in spatially extended systems. A reason for some dissatisfaction is the fact that these examples relate to nonautonomous systems, with time-dependent coefficients in the partial differential equations. It would be interesting to discover *autonomous* extended systems manifesting the hyperbolic chaos. Elaboration of such an example is the goal of the present article; we will present an autonomous set of nonlinear partially differential equations manifesting an attractor of Smale – Williams type in the Poincaré map. At the moment we do not pretend to relate this construction to a concrete physical system, but we suppose that it may be implementable, in particular, on the basis of electronic circuits (say, in a kind of nonlinear transmission line).

2. THE MAIN MODEL AND RESULTS OF COMPUTER SIMULATION

Following [11], let us start with the one-dimensional Swift – Hohenberg equation

$$\partial_t u + (1 + \kappa^2 \partial_x^2)^2 u = \mu u - u^3. \tag{2.1}$$

A trivial solution of this equation $u \equiv 0$ becomes unstable at $\mu > 0$. In linear approximation, substituting $u \sim \exp(\lambda t - ikx)$, we evaluate the increment of the perturbation as $\lambda = \mu - \left(1 - \kappa^2 k^2\right)^2$. It is maximal at $k = k_0 = 1/\kappa$ that corresponds roughly to the wave number of the Turing pattern, which grows up from arbitrarily small random initial perturbations in the medium. Due to the cubic nonlinear term in (2.1) the pattern, which is nearly periodic in space, saturates at some finite level of magnitude.

To modify the model, we add one more variable v depending on the spatial coordinate x and time t, and turn to the following set of equations

$$\begin{aligned} &\partial_t u + (1 + \partial_x^2)^2 u = \mu\, u + u^3 - \tfrac{1}{5} u v^2 + \varepsilon\, v \cos 3x, \\ &\partial_t v = -v + u^2 v + u^2. \end{aligned} \tag{2.2}$$

For our purposes it is appropriate to postulate the circular geometry of the medium:

$$u(x + L, t) = u(x, t),\ \ v(x + L, t) = v(x, t), \tag{2.3}$$

where L is the system length.

The first relation in (2.2) is the modified Swift – Hohenberg equation (with inverse sign of the cubic nonlinear term), and with added terms, containing the variable v governed by the second equation. The evolution rule for the variable v is local (spatial derivatives are ignored). The term proportional to $\varepsilon \cos 3x$ implies periodic spatially inhomogeneity of coupling between the two components involved in the dynamics. In accordance with the boundary conditions, the functions u and v are spatially periodic and may be represented by Fourier series expansions.

Qualitatively, the functioning of the systems may be explained as follows. Suppose for an instant that the multiplier $\mu + u^2 - \frac{1}{5}v^2$ in the first equation (2.2) is positive; hence, the variable u grows, and it gives rise to a spatial pattern of wave-number about k_0=1. The most significant is the contribution of the first spatial harmonic component, which is characterized naturally by some phase φ: $u \approx U_1 \cos(x + \varphi)$. After a while, due to the growth of the pattern magnitude, the coefficient $(-1 + u^2)$ in the second equation becomes positive (except for narrow spatial neighborhoods of nodes of the pattern), and then the amplitude of the variable v starts to grow. In the function v the second spatial harmonic component is relevant, and at the initial stage of this instability it accepts the doubled spatial phase 2φ as it is stimulated by the quadratic nonlinear term u^2 in the second equation (2.2). So, we have $v \approx V_0 + V_2 \cos(2x + 2\varphi)$. Next, as the magnitude of v becomes large, the factor $\mu + u^2 - \frac{1}{5}v^2$ turns out to be negative. The magnitude of u starts to decrease, and consequently, the amplitude of v decreases too. This process continues until the factor $\mu + u^2 - \frac{1}{5}v^2$ becomes positive once more, and the variable u starts to grow again. The excitation of the first subsystem at this stage is stimulated by the term composed as a product of the second harmonic component of v and the function $\varepsilon \cos 3x$ with spatial inhomogeneity taken into account. It provides a transfer of the doubled spatial phase back to the pattern of u (with the opposite sign), as follows from the relation $\cos(2x + 2\varphi) \cos 3x = \cos(x - 2\varphi)/2 + \ldots$. Then, the process repeats itself over and over again. So, the spatial phases at successive stages of the pattern formation evolve according to the expanding circle map $\varphi_{n+1} = -2\varphi_n + \text{const}$. This is a chaotic map (the Bernoulli map) characterized by the positive Lyapunov exponent $\Lambda = \ln 2 = 0.693\ldots$.

Numerical simulation of the dynamics was performed at $\mu = 0.03, \varepsilon = 0.03, L = 2\pi$ using an explicit-implicit difference scheme on a grid with temporal and spatial steps, respectively, $\Delta t = 0.001, \Delta x = L/64 \approx 0.098$. One can observe relatively long-time stages of growth of the patterns, which alternate with their fast decay almost to zero (Fig. 2). The mean time period between the successive stages of excitation in this regime according to the computations is $\tau \approx 50.37$.

To analyze the chaotic behavior of the patterns, it is appropriate to deal with harmonic components of the spatial Fourier series expansions for $u(x, t)$ and $v(x, t)$. The complex amplitudes of the Fourier components were evaluated numerically in the course of the integration of the equations at each time step. In Fig. 3 the diagrams (a)–(f) show the amplitudes of the harmonic components, U_1, U_3, and V_0, V_2, V_4, V_6, on a time interval of ten characteristic periods of the dynamics. Note that the magnitude of U_1 just before the drops is much larger than that of the third harmonic component U_3. The magnitudes of the Fourier components V_0, V_2 and V_4 are roughly of the same order. The even components of u and odd components of v are of negligible small amplitude.

An important observation is that the spatial phases of the patterns at successive stages of activity evolve chaotically, as seen from Figs. 2 and 3. To analyze the dynamics of the phases in the computations, we apply the Poincaré section technique. An appropriate selection for the surface of the cross-section in the state space of the system is determined by the condition that the amplitude of the first harmonic component U_1 decreasing in time passes the value 1, i.e., satisfies the equality $S = |U_1| - 1 = 0$.

Figure 4 shows an iteration diagram for the spatial phases of the pattern $u(x, t)$ computed as values of the argument of the complex amplitude U_1 at successive passages of the Poincaré section and portrait of the attractor in the Poincaré section in two-dimensional projection onto a plane of real and imaginary parts of U_1. As seen from panel (a), the dynamics of the spatial phase correspond to the expanding circle map (the Bernoulli map). Indeed, one complete round from 0 to 2π for the preimage φ_n corresponds to two rounds for the image φ_{n+1} (in the reverse direction).

For the sustained chaotic regime we computed Lyapunov exponents for the Poincaré map. It was done using the Benettin algorithm adapted for the distributed system [9, 14–16], with Gram – Schmidt orthogonalization of the perturbation vectors corresponding to a restricted number of modes of spatially depending variations near the analyzed pattern evolving in time. At $\mu = 0.03$, $\varepsilon = 0.03$, $L = 2\pi$ the first four exponents (from the infinite spectrum of those in the distributed system) are $\Lambda = \{0.665, -42.26, -44.51, -46.46, \ldots\}$. The largest Lyapunov exponent for the Poincaré map is remarkably close to the value $\ln 2$ corresponding to the uniformly expanding circle map. Other exponents are negative.

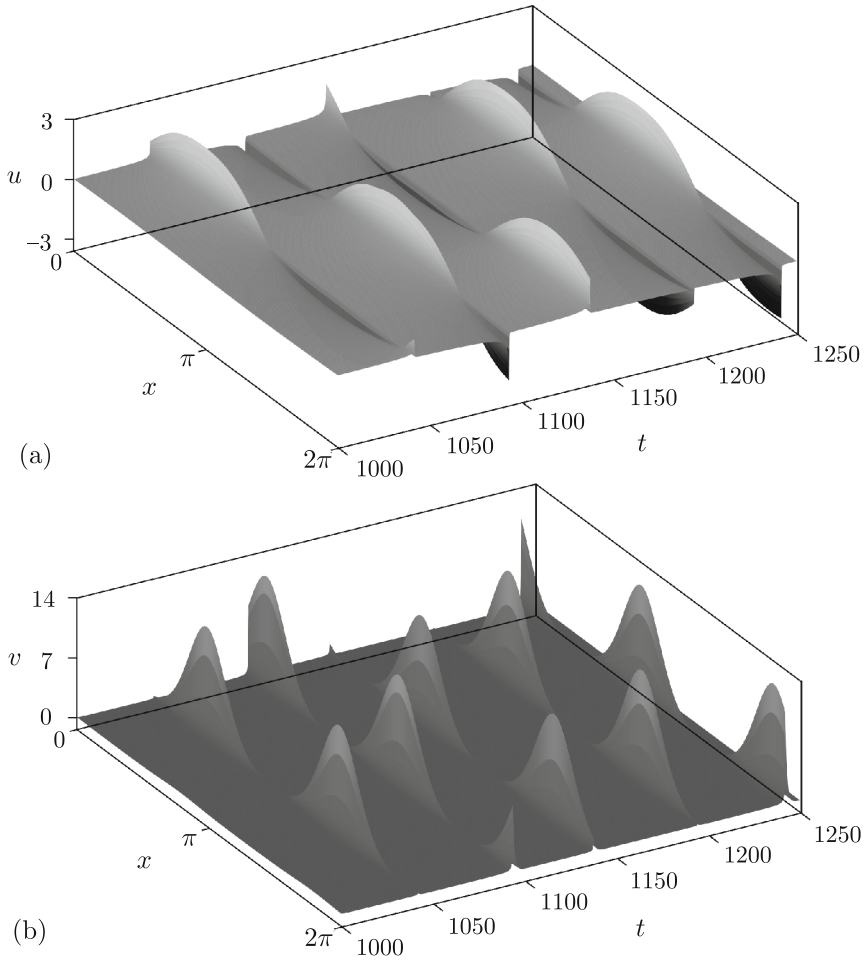

Fig. 2. Spatio-temporal plots for the variables $u(x, t)$ (a) and $v(x, t)$ (b) obtained from the numerical solution of equations (2.2) with periodic boundary conditions at $\mu = 0.03$, $\varepsilon = 0.03$, $L = 2\pi$.

Summarizing, we conclude that in the state space of the system there is a twofold expansion of a phase-volume element along some circular variable (that is the spatial phase of the pattern) accompanied by compression in other directions. It means that we deal with an attractor that is a kind of Smale – Williams solenoid embedded in the (infinite-dimensional) state space of the Poincaré map of our system. The estimate of the Kaplan – Yorke dimension based on the spectrum of the Lyapunov exponents yields $D_{KY} \approx 1.016$. The fractional part of the dimension is rather small because of strong transversal compression of the phase volume near the attractor.

3. THE 5D MODEL

Having in mind that the functioning of the system according to the above qualitative explanation is based on the interaction of spatial Fourier harmonics, one can try to reduce the dynamics to finite-dimensional ordinary differential equations for amplitudes of the most significant modes of the components u and v.

The simplest set of shortened equations, which correctly reflects the qualitative character of the dynamics, may be derived by substitution of the following ansatz:

$$u = U_1 e^{ix} + U_1^* e^{-ix}, \; v = w + V_2 e^{2ix} + V_2^* e^{-2ix}. \tag{3.1}$$

Here $U_1(t)$ is the complex amplitude of the first harmonic of the function u, $V_2(t)$ is the complex amplitude of the second harmonic of the function v, and $w(t)$ is a real variable corresponding to the spatially independent component of v. With this substitution in (2.2), multiplying the first

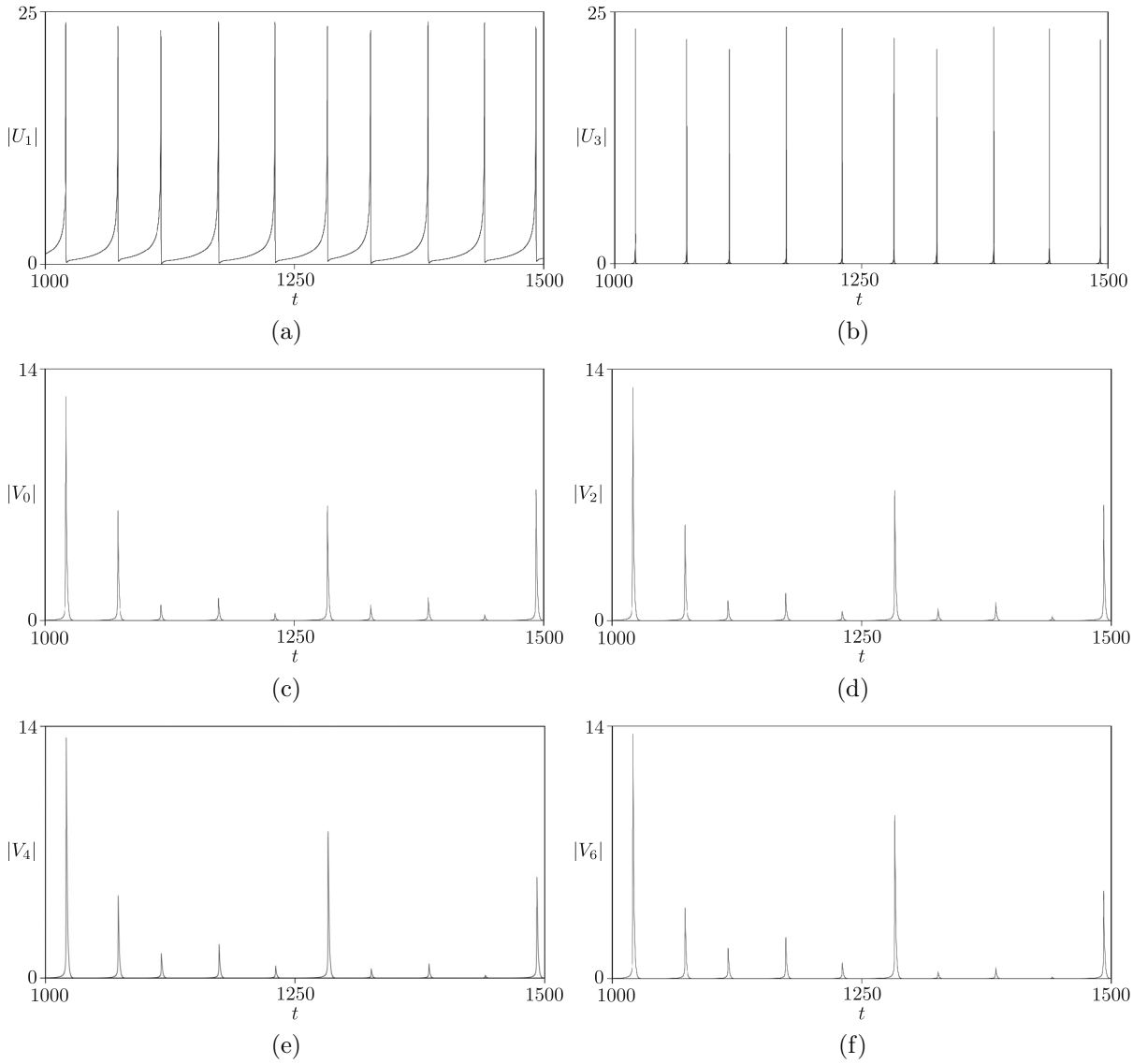

Fig. 3. Absolute values of the amplitudes of the spatial Fourier components U_1, U_3 and V_0, V_2, V_4, V_6 for the variables u and v versus time as obtained from numerical solution of (2.2), (2.3) at $\mu = 0.03$, $\varepsilon = 0.03$, $L = 2\pi$.

equation by e^{-ix}, and the second by e^{-2ix} or 1, after averaging over a spatial period 2π, we arrive at the following set of equations

$$\begin{aligned} \dot{U}_1 &= \left(\mu - \frac{1}{5}w^2 + 3|U_1|^2 - \frac{2}{5}|V_2|^2\right) U_1 - \frac{2}{5}V_2 U_1^* w + \frac{1}{2}\varepsilon V_2^*, \\ \dot{V}_2 &= (2|U_1|^2 - 1)V_2 + (w+1)U_1^2, \\ \dot{w} &= -w + 2\mathrm{Re}(V_2 U_1^{*2}) + 2|U_1|^2(w+1). \end{aligned} \tag{3.2}$$

Figure 5 illustrates some results of numerical solution of (3.2) by the Runge – Kutta fourth-order method. Here the time dependences are plotted for amplitudes and arguments of the complex variables U_1 and V_2 and for the real variable w. One can see that the plots look similar to those corresponding to the original partial differential equations. Jumps on the plots for the phases correspond to short time intervals of transfer of the excitation between the spatial modes as explained.

To construct numerically the Poincaré map, we select the surface of the cross-section by the relation $S = |U_1| - 1 = 0$ and consider the variables at the instants when the orbits cross this

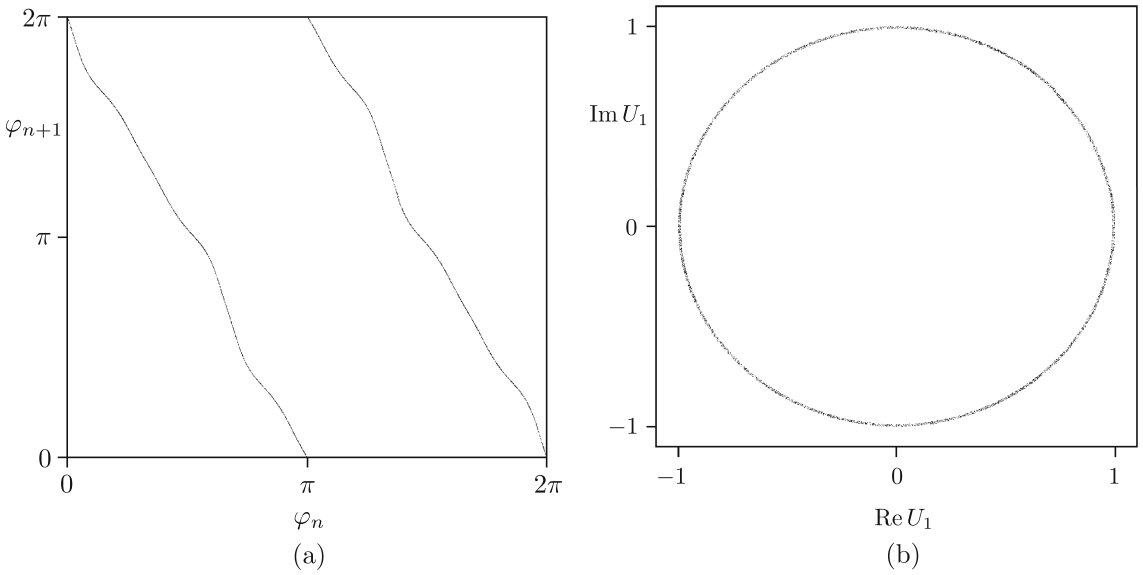

Fig. 4. Diagram for spatial phases of the patterns for the variable u evaluated as arguments of the complex amplitude of the first spatial harmonic U_1 at successive crossing of the Poincaré section (a) and projection of the attractor in the Poincaré section onto the plane of real and imaginary parts of U_1 (b) at $\mu = 0.03$, $\varepsilon = 0.03$, $L = 2\pi$.

surface in the direction of decrease of U_1. For the five-dimensional autonomous set of Eqs. (3.2) the Poincaré map is four-dimensional. Figure 5a shows a diagram for the phases of the variable U_1 at successive crossing of the surface of the Poincaré section at $\mu = 0.03$, $\varepsilon = 0.03$. As can be seen, the dynamics of the phases in the low-dimensional model is governed by the expanding circle map for the phases, although undulating is much more pronounced on the curve than that in the original model. Figure 5b shows the attractor in the Poincaré cross-section in projection onto a plane of real and imaginary parts of U_1. For this attractor we computed the Lyapunov exponents for the Poincaré map by the Benettin algorithm with Gram – Schmidt orthogonalization of the perturbation vectors around the reference orbit on the attractor, they are $\Lambda = \{0.65, -46.95, -49.57, -51.14\}$. The mean period of the passage between the successive crossings of the Poincaré section was found to be $\tau \approx 52.61$. Note that the largest Lyapunov exponent is close to $\ln 2$, and the others are negative. It corresponds to the attractor of Smale – Williams type in the four-dimensional state space of the Poincaré map. The estimate of the fractal dimension according the Kaplan – Yorke formula yields $D_{KY} \approx 1.014$.

4. THE 7D MODEL

To obtain more accurate finite-dimensional models of larger phase space dimension, one can increase the number of spatial Fourier components that are taken into account. The system (3.2) is a model with the minimal number of dynamical variables which captures the main features of the dynamics, but quantitatively the description becomes much better in the seven-dimensional model. Let us use instead of (3.1) the following substitution

$$u = U_1 e^{ix} + U_1^* e^{-ix}, \quad v = w + V_2 e^{2ix} + V_2^* e^{-2ix} + V_4 e^{4ix} + V_4^* e^{-4ix}, \tag{4.1}$$

where V_4 is the complex amplitude of the fourth spatial Fourier component of the variable $v(x, t)$.

Then, from the manipulations similar to those in derivation of the model (3.2), we obtain the set of ordinary differential equations

$$\begin{aligned}
\dot{U}_1 &= \left(\mu - \frac{1}{5}w^2 + 3|U_1|^2 - \frac{2}{5}|V_2|^2 - \frac{2}{5}|V_4|^2\right) U_1 - \frac{2}{5}V_2 U_1^* w - \frac{2}{5}U_1^* V_2^* V_4 + \frac{1}{2}\varepsilon(V_2^* + V_4), \\
\dot{V}_2 &= (2|U_1|^2 - 1)V_2 + V_4 U_1^{*2} + (w+1)U_1^2, \\
\dot{V}_4 &= (2|U_1|^2 - 1)V_4 + U_1^2 V_2, \\
\dot{w} &= -w + 2Re(V_2 U_1^{*2}) + 2|U_1|^2(w+1).
\end{aligned} \tag{4.2}$$

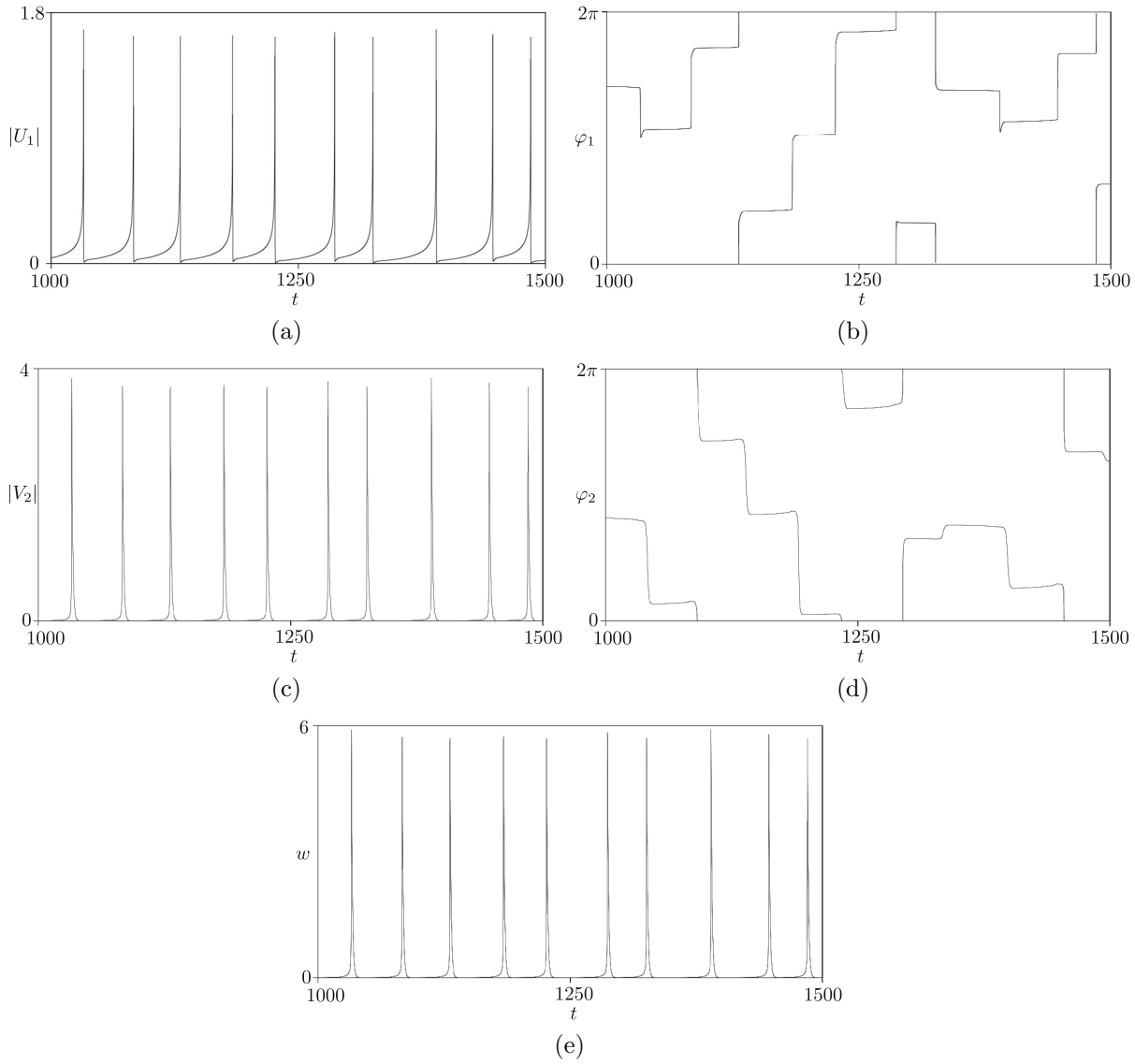

Fig. 5. Time dependences for amplitudes and phases of the complex variables U_1 and V_2 and for the real variable w obtained from the numerical solution of (3.2) $\mu = 0.03$, $\varepsilon = 0.03$.

(We ignore additional harmonics in the Fourier expansion for the function $u(x, t)$ as they appear to have small amplitudes and do not influence notably the accuracy of the description.)

Figure 7 illustrates numerical results obtained for the model (4.2) at $\mu = 0.03$, $\varepsilon = 0.03$; the time dependences are plotted for the amplitudes and arguments of U_1, V_2, V_4 and for the real variable w. Using the relation $S = |U_1| - 1 = 0$ and considering the variables at the crossing of this surface by the orbits in the direction of decrease of U_1 we construct the Poincaré map, which is six-dimensional for this model. Figure 8a shows the diagram for the phases of U_1 at the successive crossing of the surface of the Poincaré section. It corresponds to the expanding circle map, like in the main model of Section 2 and in the low-dimensional model of Section 3. Observe that the undulating in the plot has decreased essentially in comparison with the five-dimensional model, and the form corresponds much better to the original distributed system (cf. Fig. 4a). Figure 8b shows the attractor in the Poincaré cross-section in projection onto a plane of real and imaginary parts of U_1.

Lyapunov exponents for the Poincaré map computed by the Benettin algorithm with Gram-Schmidt orthogonalization are $\Lambda = \{0.67,\ -41.72,\ -46.34,\ -47.35,\ -47.62,\ -47.81\}$. Observe the better agreement with the exponents of the distributed model in comparison with the five-dimensional model. The mean period of the passages between successive crossings of the Poincaré

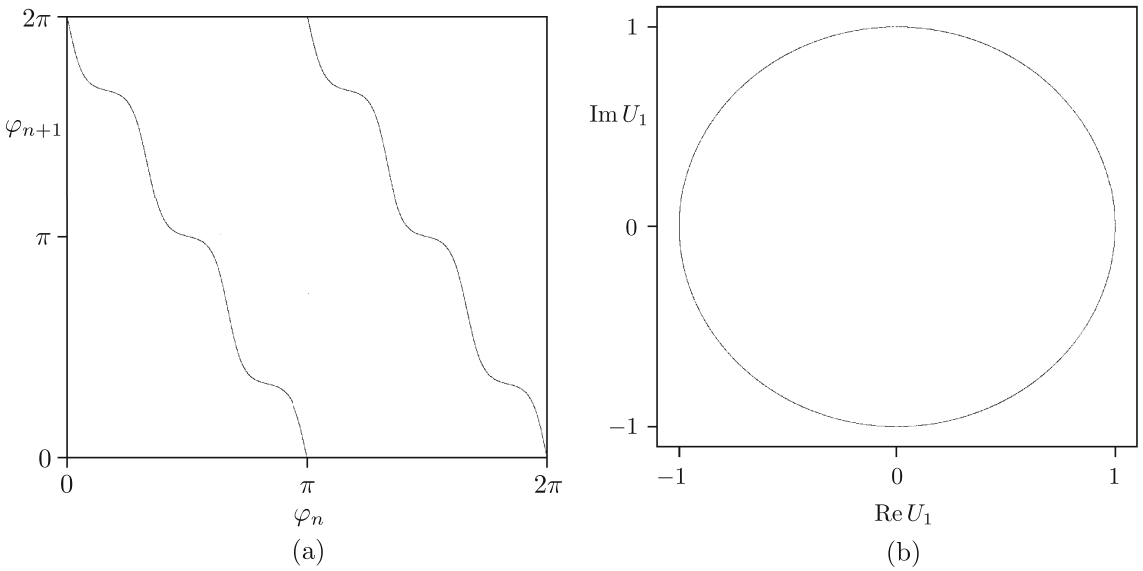

Fig. 6. Diagram for phases of the complex variable U_1 at successive crossing of the Poincaré section (a) and projection of the attractor in the Poincaré section onto the plane of real and imaginary parts of U_1 (b) for the 5D-model (3.2) at $\mu = 0.03$, $\varepsilon = 0.03$.

section in this regime was found to be $\tau \approx 49.6$. Again we see that the largest Lyapunov exponent is close to $\ln 2$, and the others are negative, which corresponds to the attractor of Smale – Williams type embedded in the six-dimensional state space of the Poincaré map. The estimate of the fractal dimension according to the Kaplan – Yorke formula yields $D_{KY} \approx 1.016$, which agrees well with the distributed model.

5. HYPERBOLICITY TEST FOR THE FINITE-DIMENSIONAL MODELS

For attractors of the 5D and 7D models discussed in the two previous sections, we have conducted a numerical test for hyperbolicity following the approach suggested in [17, 18] and applied to hyperbolic attractors in [6–9].

The method is based on the estimate of distribution of angles between stable and unstable manifolds on the attractor. The stable and unstable manifolds for the hyperbolic attractor can meet only with nonzero angle; the touches must be excluded. (Their presence would signalize the nonhyperbolic nature of the attractor, see, e.g., [9] for examples.) The procedure consists in computing the vectors of small perturbations along a representative trajectory on the attractor in forward and inverse time, and in measuring the angles between the forward-time vectors and the spanned subspace of vectors unstable in the backward-time at crossings of the Poincaré section by the reference trajectory. In our case the unstable manifold is one-dimensional, and the stable manifold is of dimension $N - 1$, where $N = 4$ or 6 is the phase space dimension for the Poincaré map. Instead of tracing all relevant vectors in the backward-time, in the computations one can deal with only one vector generated by the *conjugate* linear equations for perturbations at the reference trajectory; see details in Ref. [19], where this modification of the method was suggested. If zero values of the angle do not occur, i.e., the statistical distribution of the angles is separated from zero, one concludes that the dynamics is hyperbolic. If the statistics show nonvanishing probability for zero angles, it implies nonhyperbolic behavior because of the presence of the homoclinic tangencies of the stable and unstable manifolds.

In our 5D and 7D models we first generate a sufficiently long representative orbit on the attractor from the numerical solution of Eqs. (3.2) or (4.2). Then we integrate numerically the linearized variation equations forward in time to get a perturbation vector $\mathbf{a}(t)$ normalizing it at each step of integration to exclude the divergence. This vector determines an unstable direction at each point of the orbit. Next, we solve the conjugate linearized variation equations along the same reference trajectory in backward time to get a vector $\mathbf{v}(t)$ orthogonal to the three-dimensional stable subspace. Then we compute an angle $\beta \in [0, \pi/2]$ between $\mathbf{v}(t)$ and $\mathbf{a}(t)$ from the relation $\cos\beta = |\mathbf{v}(t) \cdot \mathbf{a}(t)|/|\mathbf{v}(t)||\mathbf{a}(t)|$ and set $\alpha = \beta - \pi/2$.

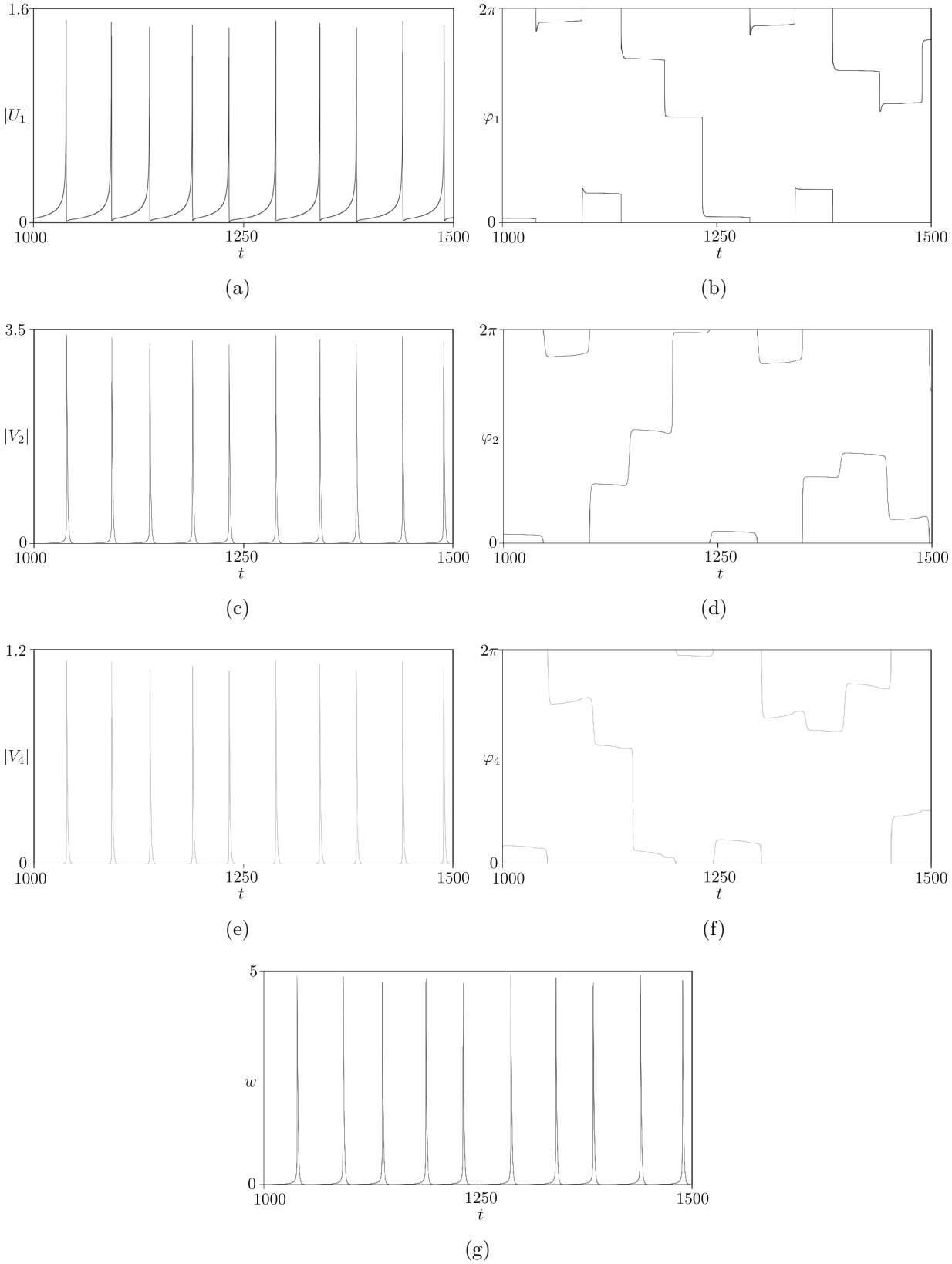

Fig. 7. Time dependences for amplitudes and phases of the complex variables U_1, V_2, V_4 and for the real variable w obtained from numerical solution of (4.2) at $\mu = 0.03$, $\varepsilon = 0.03$.

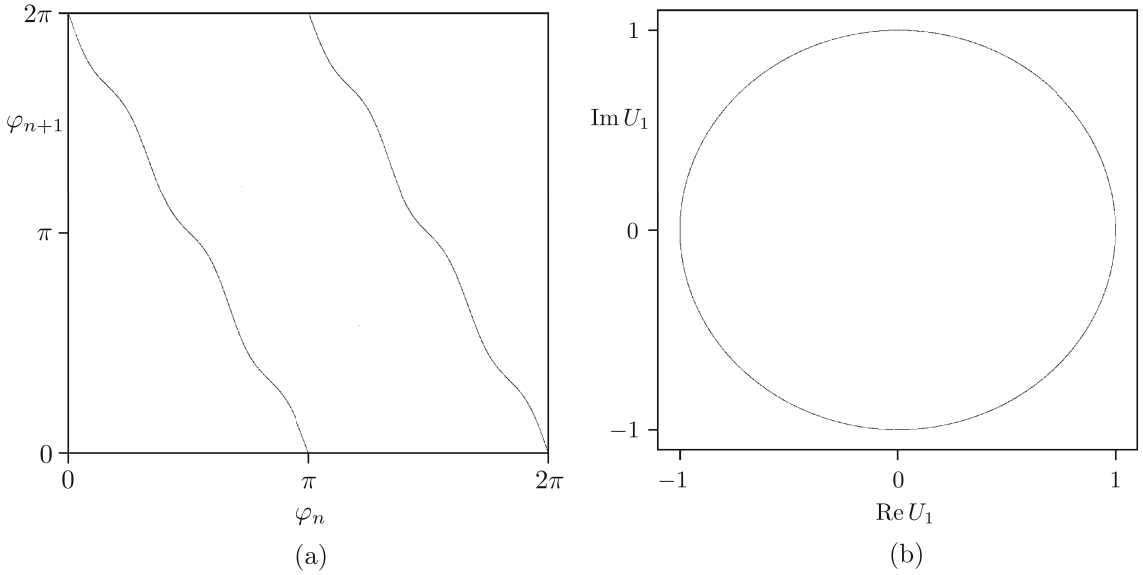

Fig. 8. Diagram for the phases of the complex variable U_1 at the successive crossing of the Poincaré section (a) and projection of the attractor in the Poincaré section onto the plane of real and imaginary parts of U_1 (b) for the 7D-model (4.2) at $\mu = 0.03$, $\varepsilon = 0.03$.

Figure 9 shows histograms for distributions of the angles α obtained in computations for the 5D and 7D models at $\mu = 0.03$ and $\varepsilon = 0.03$. Observe the clearly visible separation of the distributions from zero values of the angles. So, the test confirms the hyperbolicity of the attractors.

6. CONCLUSION

In this article, we have discussed an example of the autonomous distributed system with ring geometry (periodic boundary condition), which implements chaotic dynamics corresponding to a uniformly hyperbolic attractor, a kind of Smale – Williams solenoid in the Poincaré map. The dynamics consists of sequential birth and death of the spatial patterns; the Smale – Williams attractor occurs due to the fact that the spatial phases of these patterns at each next stage of activity are transformed according to the doubly expanding circle map. Also, we have derived and studied numerically the truncated models represented by a five-dimensional and a seven-dimensional set of ordinary differential equations. Their dynamics are found to correspond qualitatively to the original distributed system. For these models, the hyperbolicity of the attractor is confirmed by a computer-based test, which indicates the lack of touches for stable and unstable manifolds of the orbits on the attractor.

Thus, we get the first example of an autonomous distributed system with a uniformly hyperbolic attractor. As believed, it revives the old hope that such attractors may be relevant to some cases of complex dynamics of spatially extended systems (like the hydrodynamic turbulence). We can assume that the system considered may be implemented in electronics based on a kind of nonlinear transmission line. The attractiveness of systems with uniformly hyperbolic attractors in the framework of possible practical application of chaos is determined by their structural stability or robustness: the generated chaos is insensitive to variations of parameters, imperfection of fabrication, technical fluctuations in the system, etc.

ACKNOWLEDGMENTS

This work was supported by RFBR grant No 11-02-91334 and DFG grant No PI 220/14-1. V. P. K. acknowledges support from DAAD in the framework of the program Forschungsstipendien für Doktoranden und Nachwuchswissenschaftler.

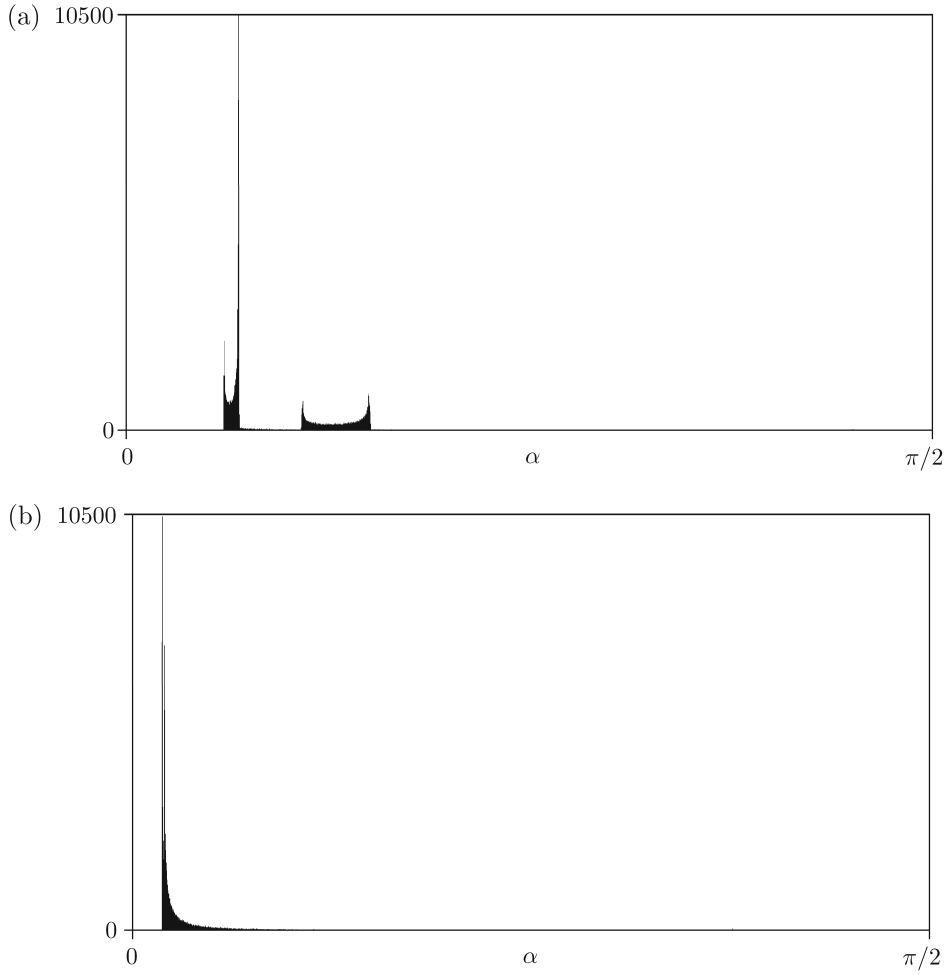

Fig. 9. Histograms for distributions of the angles between the stable and unstable subspaces on the attractors for the models of dimension 5 (a) and 7 (b) obtained in computations at $\mu = 0.03$, $\varepsilon = 0.03$.

REFERENCES

1. Smale, S., Differentiable Dynamical Systems, *Bull. Amer. Math. Soc. (NS),* 1967, vol. 73, pp. 747–817.
2. Williams, R. F., Expanding Attractors, *Publ. Math. Inst. Hautes Études Sci.,* 1974, vol. 43, pp. 169–203.
3. Shilnikov, L., Mathematical Problems of Nonlinear Dynamics: A Tutorial, *Internat. J. Bifur. Chaos Appl. Sci. Engrg.,* 1997, vol. 7, no. 9, pp. 1953–2001.
4. *Dynamical Systems 9: Dynamical Systems with Hyperbolic Behaviour,* D. V. Anosov (Ed.), Encyclopaedia Math. Sci., vol. 9, Berlin: Springer, 1995.
5. Plykin, R. V. and Klinshpont, N. E., Strange Attractors: Topologic, Geometric and Algebraic Aspects, *Regul. Chaotic Dyn.,* 2010, vol. 15, nos. 2–3, pp. 335–347.
6. Kuznetsov, S. P., Example of a Physical System with a Hyperbolic Attractor of the Smale – Williams Type, *Phys. Rev. Lett.,* 2005, vol. 95, no. 14, 144101, 4 pp.
7. Kuznetsov, S. P. and Pikovsky, A., Autonomous Coupled Oscillators with Hyperbolic Strange Attractors, *Phys. D,* 2007, vol. 232, no. 2, pp. 87–102.
8. Kuznetsov, S. P., Example of Blue Sky Catastrophe Accompanied by a Birth of Smale – Williams Attractor, *Regul. Chaotic Dyn.,* 2010, vol. 15, nos. 2–3, pp. 348–353.
9. Kuznetsov, S. P., *Hyperbolic Chaos: A Physicist's View,* Berlin: Springer, 2012.
10. Kuznetsov, S. P., Dynamical Chaos and Uniformly Hyperbolic Attractors: From Mathematics to Physics, *Phys. Uspekhi,* 2011, vol. 54, no. 2, pp. 119–144; see also: *Uspekhi Fiz. Nauk,* 2011, vol. 181, pp. 121–149.
11. Kuptsov, P. V., Kuznetsov, S. P., and Pikovsky, A., Hyperbolic Chaos of Turing Patterns, *Phys. Rev. Lett.,* 2012, vol. 108, no. 19, 194101, 4 pp.
12. Isaeva, O. B., Kuznetsov, A. S., and Kuznetsov, S. P., Hyperbolic Chaos of Standing Wave Patterns Generated Parametrically by a Modulated Pump Source, *Phys. Rev. E,* 2013, vol. 87, no. 4, 040901(R), 4 pp.

13. Isaeva, O. B., Kuznetsov, A. S., and Kuznetsov, S. P., Hyperbolic Chaos in Parametric Oscillations of a String, *Nelin. Dinam.,* 2013, vol. 9, no. 1, pp. 3–10 (Russian).
14. Benettin, G., Galgani, L., Giorgilli, A., and Strelcyn, J.-M., Lyapunov Characteristic Exponents for Smooth Dynamical Systems and for Hamiltonian Systems: A Method for Computing All of Them: P. 1: Theory; P. 2: Numerical Application, *Meccanica,* 1980, vol. 15, pp. 9–30.
15. Politi, A., Lyapunov Exponent, *Scholarpedia,* 2013, vol. 8, no. 3, 2722.
16. Ruffo, S., Lyapunov Spectra in Spatially Extended Systems, in *Cellular Automata and Complex Systems (Santiago, 1996),* Nonlinear Phenom. Complex Systems, vol. 3, Dordrecht: Kluwer, 1999, pp. 153–180.
17. Lai, Y.-Ch., Grebogi, C., Yorke, J. A., and Kan, I., How Often Are Chaotic Saddles Nonhyperbolic?, *Nonlinearity,* 1993, vol. 6, no. 5, pp. 779–797.
18. Anishchenko, V. S., Kopeikin, A. S., Kurths, J., Vadivasova, T. E., and Strelkova, G. I., Studying Hyperbolicity in Chaotic Systems, *Phys. Lett. A,* 2000, vol. 270, no. 6, pp. 301–307.
19. Kuptsov, P. V., Fast Numerical Test of Hyperbolic Chaos, *Phys. Rev. E,* 2012, vol. 85, no. 1, 015203(R), 4 pp.